

Is low-temperature fission-track annealing in apatite a thermally controlled process?

Murat Taner Tamer¹ and Richard A Ketcham¹

¹University of Texas at Austin

November 23, 2022

Abstract

We report a new series of experiments to explore the phenomenon of low-temperature annealing of fission tracks in apatite that feature a number of improvements over previous work. Grain mounts were pre-irradiated Cf to increase confined track detection and allow briefer thermal neutron irradiation. We co-irradiated and etched four apatite varieties (Durango, Fish Canyon, Renfrew, Tioga) over five time steps equally spaced from 3.66 to 15 ln(s). A length standard was co-etched with all experiments to ensure that subtle differences are within detection limits. Finally, we used a standard etching protocol, allowing the data to be co-modeled with extensive high-temperature data sets and recent analyses of induced tracks that underwent ambient-temperature annealing over year-to-decade time scales. Ambient-temperature annealing occurs at two different rates, with faster annealing at early stages that decreases to a slower rate that converges with empirical fanning linear or curvilinear models. The nature of this decrease varies among the apatite species examined, but no patterns could be determined. The fitted models make geological time-scale predictions consistent with those based on high-temperature data only, and also make predictions consistent with reasonable inferred low-temperature histories for all four apatite varieties. The empirical fanning curvilinear equation encompasses low-temperature annealing at month-to-decade time scales, but low-temperature annealing at shorter time scales may occur by a distinct mechanism. We consider but rule out annealing by radiation from short-lived activated isotopes. We also reconsider the notion of the initial track length, and the appropriate length for normalizing confined track length measurements.

Hosted file

supporting information in template.docx available at <https://authorea.com/users/543381/articles/601731-is-low-temperature-fission-track-annealing-in-apatite-a-thermally-controlled-process>

1 **Is low-temperature fission-track annealing in apatite a thermally controlled process?**

2 **M. T. Tamer¹, and R. A. Ketcham¹**

3 ¹Department of Geological Sciences, Jackson School of Geoscience, University of Texas,
4 Austin, TX, USA.

5 Corresponding author: Richard Ketcham (ketcham@jsg.utexas.edu)

6 **Key Points:**

- 7 • We document apatite fission-track annealing at earth-surface conditions in the seconds to
8 decades after track formation.
- 9 • Empirical annealing equations encompass most low- and high-temperature experimental
10 data, indicating that the same processes control both.
- 11 • There is evidence of a distinct annealing process operating during the seconds after
12 induced track formation.
13

14 **Abstract**

15 We report a new series of experiments to explore the phenomenon of low-temperature annealing
16 of fission tracks in apatite that feature a number of improvements over previous work. Grain
17 mounts were pre-irradiated ²⁵²Cf to increase confined track detection and allow briefer thermal
18 neutron irradiation. We co-irradiated and etched four apatite varieties (Durango, Fish Canyon,
19 Renfrew, Tioga) over five time steps equally spaced from 3.66 to 15 ln(s). A length standard
20 was co-etched with all experiments to ensure that subtle differences are within detection limits.
21 Finally, we used a standard etching protocol, allowing the data to be co-modeled with extensive
22 high-temperature data sets and recent analyses of induced tracks that underwent ambient-
23 temperature annealing over year-to-decade time scales. Ambient-temperature annealing occurs at
24 two different rates, with faster annealing at early stages that decreases to a slower rate that
25 converges with empirical fanning linear or curvilinear models. The nature of this decrease varies
26 among the apatite species examined, but no patterns could be determined. The fitted models
27 make geological time-scale predictions consistent with those based on high-temperature data
28 only, and also make predictions consistent with reasonable inferred low-temperature histories for
29 all four apatite varieties. The empirical fanning curvilinear equation encompasses low-
30 temperature annealing at month-to-decade time scales, but low-temperature annealing at shorter
31 time scales may occur by a distinct mechanism. We consider but rule out annealing by radiation
32 from short-lived activated isotopes. We also reconsider the notion of the initial track length, and
33 the appropriate length for normalizing confined track length measurements.

34 **Plain Language Summary**

35 We present a new series of experiments to study the extent to which the radiation damage from
36 fission decay of uranium in the mineral apatite is annealed (healed) at room temperature. We
37 combine data obtained by etching fission tracks seconds after being generated in a nuclear
38 reactor with tracks etched minutes, hours, days, months, years, and even decades after
39 generation, and find that detectable annealing occurs over these time spans. We combine these
40 data with previous experiments conducted at high temperatures to see whether the model
41 equations currently used to describe high-temperature annealing can encompass the low-
42 temperature data, which would support the idea that the same atomic-scale processes control
43 both. We find that most of our low-temperature data are consistent with the high-temperature
44 data and model equations, with the exception of earliest-stage experiments that show faster-than-
45 expected annealing, possibly caused by a different process. We consider but reject a possible
46 annealing effect from secondary radiation. These data make it clear that a truly “unannealed”
47 track length is unmeasurable, which in turn requires that we reconsider how we normalize
48 measurements of annealed lengths. Our measurements also allow us to more confidently
49 characterize fission-track annealing at earth-surface conditions over geological time scales.

50 **1 Introduction**

51 Fission decay results in charged particles as disintegration products, whose interactions
52 with surrounding crystalline material result in damage trails called fission tracks (Silk & Barnes,
53 1959), which can be hosted in extra-terrestrial (Fleischer et al., 1967) and terrestrial minerals
54 (Price & Walker, 1963). With suitable etching procedures these tracks become observable under
55 optical microscopes (Fleischer et al., 1965b). Fission tracks can be generated by spontaneous
56 fission of ²³⁸U and accumulate over geological time, or induced by thermal neutron irradiation of
57 ²³⁵U in nuclear reactors (Meitner & Frisch, 1939). Depending on the host material and time and

58 temperature conditions, the displaced atoms undergo reconstruction (Fleischer et al., 1965a),
59 resulting in progressive and eventually complete fading of fission tracks, which is called
60 annealing (Fleischer & Price, 1964). Progressive annealing allows fission tracks to carry
61 information on the time and temperature conditions experienced by the host material from the
62 moment of generation until etching, which can be accessed using fission track lengths. Apatite is
63 one of the most investigated minerals for fission track thermochronology (Naeser, 1967; Wagner,
64 1968) due to its abundance in various rocks and geological environments, ability to concentrate
65 sufficient amounts of U, and its straightforward etching procedure (Donelick et al., 2005).

66 Spontaneous tracks in apatite are shorter than freshly generated induced tracks in all
67 cases, even in samples with no significant geological heating (Gleadow et al., 1986; Green, 1988;
68 Jonckheere, 2003; Spiegel et al., 2007; Vrolijk et al., 1992), suggesting that annealing occurs at
69 ambient Earth surface temperatures. Length reduction at ambient temperatures has also been
70 documented in induced tracks at laboratory time scales from minutes to years after irradiation
71 (Donelick et al., 1990; Tamer et al., 2019). It remains unclear, however, whether this ambient-
72 temperature annealing reflects the same atomic scale processes that control annealing at elevated
73 temperatures, and by extension whether it can or should be characterized by the same governing
74 equations.

75 1.1 Ambient-temperature annealing at laboratory time scales

76 Evidence of track annealing at low temperatures and short time scales was reported by
77 Donelick et al. (1990) for various apatites with different chemical compositions. Two groups of
78 pre-annealed apatite mounts were irradiated at two different reactors at different thermal neutron
79 fluences ($\phi \sim 1 \times 10^{15}$ and $\sim 8 \times 10^{15}$ n/cm²) for times as brief as 37 s, and etched after waiting
80 periods ranging from 3 minutes to 125 days, mainly grouped at ~ 6 and ~ 15 ln(s), or about 10
81 minutes and 38 days, respectively. Mean confined fission-track lengths decreased measurably
82 over this period. The Donelick et al. (1990) result is consistent with spontaneous confined track
83 lengths being shorter than induced tracks in Fish Canyon Tuff (28 ± 2 Ma) apatite and Durango
84 apatite (31 ± 3 Ma), which have been assumed to have not experienced significant heating above
85 ambient earth-surface temperatures since emplacement (Gleadow et al., 1986; McDowell et al.,
86 2005). A re-analysis of the Donelick et al. (1990) data for Tioga apatite, combined with higher-
87 temperature experiments by Donelick (1991), indicates that this low-temperature annealing is
88 well described by the empirical equations used to describe fission-track annealing (e.g., Donelick
89 et al., 1999; Ketcham et al., 2007b; Laslett et al., 1987), suggesting that it may be controlled by
90 the same process. However, these data sets were generated with an etching protocol that is no
91 longer used, and the high-temperature experiments may have suffered from temperature
92 calibration issues (Carlson et al., 1999), making this result suggestive but not definitive.

93 1.2 Ambient-temperature annealing at decadal time scales

94 Previous experiments (Belton, 2006; Tamer et al., 2019) have documented low-
95 temperature annealing at decadal time scales. Annealing studies on induced tracks in apatite have
96 been conducted since the 1970's, and materials from those irradiations have been experiencing
97 ambient temperatures for up to 50 years. A recent study (Tamer et al., 2019) used such material
98 to document a ~ 0.2 μm decrease in mean track length over a time range of ~ 2 -44 years in four
99 different apatite species; additional analyses reported in this study further document these year-
100 to-decadal annealing trends.

101 1.3 This study

102 To increase our understanding of ambient-temperature length reduction, we designed a
103 study building and improving upon Donelick et al. (1990) in several ways. The first is to implant
104 ²⁵²Cf tracks into the polished surface of pre-annealed apatite grain mounts prior to neutron
105 irradiation and etching, to increase the number of induced confined tracks etched (Donelick &
106 Miller, 1991). This measure allows us to decrease the thermal neutron irradiation time and
107 commence experiments as quickly after the onset of track formation as possible. The second is to
108 irradiate more (five) aliquots to obtain more observation points to document short-term
109 annealing, with regular sampling across a larger time range. The third improvement is to etch c-
110 axis-parallel cut Durango apatite crystals containing fossil tracks along with each irradiated
111 mount, to provide an additional rigorous control on the etching quality and consistency for each
112 experiment. The fourth improvement is studying a wider kinetic range of apatite species and
113 applying a standard etching protocol (5.5 M HNO₃, 20s, 21°C) that allows us to link results to
114 more extensive high-temperature annealing data sets (Carlson et al., 1999).

115 We also assembled data documenting low-temperature annealing at decadal time scales,
116 combining new measurements on the same apatites irradiated at various times in the past with
117 literature values acquired using the identical etching procedure (Carlson et al., 1999; Tamer et
118 al., 2019).

119 Finally, we combine high- and low-temperature annealing data to fit new annealing
120 models for various apatites, and compare them with previous fits based only on high-temperature
121 experiments. This allows us to both examine whether the low-temperature data are consistent
122 with the annealing behavior implied by the high-temperature results, and the extent to which the
123 concept of “unannealed” track length used in previous studies requires reconsideration or
124 modification (cf. Laslett & Galbraith, 1996).

125 2 Materials and Methods

126 2.1 Samples

127 Table 1 lists sample details. We selected apatite species for this study using several
128 criteria. Availability of material from earlier irradiations was necessary to allow co-investigation
129 of decadal ambient temperature annealing. We also wanted apatites that had been previously
130 studied using high-T annealing experiments. Another advantage was for the natural samples to
131 have a well-studied, distinct thermal history of rapid cooling followed by solely ambient
132 temperature annealing over geological time scales, allowing us to monitor any new model
133 predictions based on corresponding spontaneous track data. Durango (DR) and Fish Canyon Tuff
134 (FC) apatite fit all three criteria, while Renfrew (RN) and Tioga (TI) apatite satisfy the first two,
135 but have not previously had thermal histories estimated. In all, 33 aliquots from these four apatite
136 species from two different fission-track laboratories (University of Texas at Austin and
137 University of Melbourne) were measured, of which 20 were irradiated for this study, nine were
138 irradiated previously, and four samples had fossil tracks. Additionally, five DR apatite samples
139 with spontaneous tracks were used as etching quality monitors.

140 **Table 1.** *Apatite specimens used in this study.*

Apatite	Locality	This study	Previous irradiations				Samples with fossil tracks	Composition (apfu) ¹		
		Apatite source ²	Apatite source ²	Irradiation location ²	Irradiation date	Track age (ln(s))	Apatite source ²	F	Cl	OH
DR	Cerro de Mercado, Durango, Mexico	UT	UT	UT	5/12/2014	18.32 ⁴	UT	1.80	0.13	0.07
			UT	TAMU	2/1/1992 ³	20.51				
			UM	UM	3/8/1990	20.56 ⁴				
			UM	UM	2/20/1985	20.74 ⁴				
FC	Fish Canyon Tuff, San Juan Mountains, Colorado, U.S.A	UT	UT	UT	5/12/2014	18.49	UT	1.12	0.23	0.65
RN	Renfrew Rensselaer Ontario, Canada	UM	UT	TAMU	2/1/1992 ³	20.51	UM	1.81	0.01	0.18
			UM	UM	3/8/1990	20.56 ⁴				
			UM	UM	2/20/1985	20.74 ⁴				
TI	Tioga ash bed near Old Port, Pennsylvania, U.S.A	UT	UT	TAMU	2/1/1992 ³	20.51	UT	0.87	0.17	0.96

141 ¹ Composition data from Carlson et al. (1999); stoichiometry calculations from Ketcham (2015). ² Location codes: TAMU=Texas
142 A&M University; UM=University of Melbourne; UT=University of Texas at Austin. ³ Date approximate within one month. ⁴ Track
143 measurement data from Tamer et al. (2019).

144 2.2 Laboratory time scale annealing experiments

145 Apatites to be irradiated were first annealed at 450°C for 48h to erase all
 146 spontaneous tracks. Five epoxy grain mounts were prepared for irradiation, each
 147 containing pre-annealed aliquots of all four apatites. The grains from different apatite
 148 species were placed in distinct parts of the mount and kept isolated from each other
 149 during preparation. The five DR apatite monitor mounts were prepared separately. After
 150 polishing to reveal internal grain surfaces, both the experimental and monitor mounts
 151 were ²⁵²Cf-irradiated ($\sim 1 \times 10^{15}$ tracks/cm²).

152 The experimental mounts were then placed in a sealed plastic container and
 153 irradiated at the University of Texas Nuclear Engineering Teaching Lab (NETL) TRIGA
 154 Mark II nuclear research reactor. A pneumatic system allowed us to load samples from a
 155 fume hood, transfer them to the reactor, and quickly retrieve them after irradiation. The
 156 samples were irradiated for 20 s with a thermal neutron fluence of $\sim 8 \times 10^{15}$ n/cm², and
 157 returned to the fume hood 10 s after irradiation. Upon arrival, the samples were extracted
 158 from the container, and within ~ 4 s one of the irradiated mounts was etched together with
 159 one of the DR monitor mounts. The sample and monitor were etched with 5.5 M HNO₃
 160 for 20 seconds at 21 °C and immersed in water immediately afterwards. The other
 161 irradiated mounts were etched together with monitors after longer intervals, as listed in
 162 Table 2.

163 **Table 2.** *Etching times and monitor measurements.*

Exp	Etching time after irradiation			Co-etched monitor data (μm)					
	s	ln(s)	Various	N	l_m	σ_{lm}	N	D_{par}	σ_{Dpar}
1	39	3.66	39 seconds	81	14.55 (07)	0.67	41	1.87 (02)	0.11
2	1098	7.00	18.3 minutes	64	14.41 (08)	0.65	35	1.85 (02)	0.10
3	21996	10.00	6.11 hours	60	14.59 (10)	0.79	40	1.82 (02)	0.11
4	162432	12.00	1.88 days	45	14.69 (09)	0.61	48	1.80 (01)	0.09
5	3269017	15.00	37.8 days	47	14.44 (09)	0.60	41	1.81 (01)	0.09

164

165 Special considerations apply for reporting the annealing interval for the first
 166 experiment. We assume that a fission track anneals from the moment it is generated until
 167 it is etched to its tips. During irradiation tracks are continuously generated, and thus some
 168 tracks experienced 20s of reactor-ambient temperatures while others were forming.
 169 Similar considerations apply for the etching time, which is different for every confined
 170 track depending on when the impinging track creating the etchant pathway enlarges
 171 sufficiently to intersect it. The total duration for the first experiment was 54 seconds: 20
 172 seconds for irradiation, 10 seconds for sample transfer, 4 seconds for sample extraction
 173 from the sealed container and 20 seconds of etching. We estimate the mean formation
 174 time as 10 seconds after the irradiation began, and mean etching completion to be 15
 175 seconds after the etch began, based on step etching experiments, resulting in an average
 176 ambient temperature annealing time for the first experiment of 39 seconds (3.66 ln(s)).

177 2.3 Decadal time scale annealing experiments

178 The annealing study by Carlson et al. (1999) included the four apatite species
 179 used in this study. Unused irradiated apatites from the Carlson et al. (1999) study have

180 experienced ~27 years of ambient-temperature annealing. We prepared additional mounts
181 of this material for each apatite species for induced track length measurements to
182 evaluate annealing over this time.

183 2.4 Measurements

184 All fission track length and etch figure length (D_{par}) measurements were carried
185 out at the Fission Track Laboratory at the Jackson School of Geosciences at the
186 University of Texas at Austin. The mounts were scanned to find the grains parallel to
187 crystallographic c-axis, and images of confined fission tracks were captured with a Zeiss
188 M2m Axio Imager microscope using TrackWorks v3 software. Length measurements on
189 the images used FastTracks v3 software.

190 3 Data analysis methods

191 3.1 C-axis projection

192 To help account for anisotropy, we first determined the most appropriate c-axis
193 projection model for our measurements. The inter-laboratory study by Ketcham et al.
194 (2015, Fig. 6) compared fitted ellipse intercepts (l_c and l_a) from measurements of four
195 induced confined track length standards for each participant with trends from two major
196 data sets acquired with different etching protocols: Carlson et al. (1999) with 5.5 M
197 HNO₃ 20s 21°C, and Barbarand et al. (2003), with 5.0 M HNO₃ 20s 20°C. They found
198 that the l_c vs. l_a slope was not dependent on etching, as previously supposed, but on
199 analyst-specific factors that have not yet been identified. A fitted regression line of our
200 measurements of the same standards exhibits a trend more similar to the Barbarand et al
201 (2003) result, and so we use the 5.0M projection model from Ketcham et al. (2007a) to
202 calculate individual and mean c-axis projected lengths for our data. We did not calculate
203 projected lengths for the Donelick et al. (1990) data due to their distinct etching protocol
204 (5.0 M HNO₃ 25s 23°C), and instead use the individually-fitted ellipse values they
205 reported.

206 Because of the low annealing level of many of our samples, some of the very long
207 lengths encountered (>18 μm) were beyond the range encompassed in the c-axis
208 projection model, causing their projected lengths to be shorter than the actual measured
209 length. For these tracks the projected length was assumed to be equal to their actual, non-
210 projected length.

211 3.2 Fitting annealing models

212 3.2.1 Background

213 All modern interpretation and modeling of fission-track data rests on the
214 assumption that spontaneous tracks annealing over geological time scales and conditions
215 can be represented adequately by induced tracks annealing at laboratory time scales and
216 conditions. A corollary assumption is that the annealing mechanism is the same in both
217 situations. Yet another assumption is that the empirical models currently used to fit
218 fission-track data reflect the underlying physical mechanism(s) sufficiently well to make
219 such extrapolations with reasonable accuracy.

220 Our new data test these assumptions in a number of ways. Because they include
221 annealing at lower temperatures over time scales both shorter and longer than any
222 included in previous annealing data sets or models, they significantly extend the range of

223 conditions that need to be encompassed. Because this extended thermal regime directly
 224 overlaps relevant geological conditions, our data relate more directly to the conditions
 225 experienced by and processes operating within geological samples. Furthermore, insofar
 226 as most annealing models are based on lengths normalized to an “unannealed” state,
 227 progressive annealing at surface temperatures raises the question of what this state is, and
 228 thus what the normalizing value should be, or mean. Most previous studies have assumed
 229 that tracks etched some number of months after irradiation can be considered unannealed
 230 for modeling purposes without significant penalty (e.g., Crowley et al., 1991; Ketcham et
 231 al., 2007b; Ketcham et al., 1999; Laslett et al., 1987).

232 This last point has additional practical implications. Measurements of mean
 233 initial track length (l_0) are typically executed 2-18 months after irradiation, after some
 234 low-temperature annealing may have taken place. Measured values vary among apatite
 235 varieties by over 1 μm (Carlson et al., 1999), enough to affect thermal history
 236 interpretation and inversion. Laslett and Galbraith (1996) explored making the
 237 normalizing value a fitted parameter (μ_{max}) in their reconsideration of data from Crowley
 238 et al. (1991), but their approach gave the non-intuitive result that two apatite varieties
 239 with measured l_0 values less than 0.1 μm apart had μ_{max} values 2.25 μm apart. Ketcham
 240 et al. (1999, Appendix B) conducted a similar exercise and got a less severe but still
 241 unsatisfying result, with fitted normalizing values from 4-14% longer than measured ones
 242 for various apatites, and no evident way to determine how large the correction should be
 243 when analyzing an unknown apatite. Ketcham et al. (2007b) also experimented with
 244 such a correction when combining the data sets of Carlson et al. (1999) and Barbarand et
 245 al. (2003) into a single annealing model, and rejected the result when identical apatites
 246 measured by different analysts gave very different corrections.

247 Given these considerations, we raise three questions to focus the present study. (1)
 248 Is ambient-temperature annealing over seconds to decades predicted by or encompassed
 249 in current annealing models? (2) Is there a reliable way to measure or estimate the true
 250 unannealed mean track length? (3) How should the normalizing value for track lengths be
 251 defined and determined?

252 3.2.2 Annealing model equations

253 The general form of the empirical annealing model is (Ketcham et al., 1999):

$$254 \quad g(l; l_0, \alpha, \beta) = f(t, T; C_i) \quad (1)$$

255 where g transforms the lengths according to the measured initial track length (l_0), and up
 256 to two fitted parameters α and β ; and f is a function of time (t), temperature (T), and a
 257 series of fitted parameters (C_i). The model fits a normalized or “reduced” track length r ,
 258 defined as l/l_0 , which is assumed to have a maximum value of one. Because we are
 259 including data from different sources (Carlson et al., 1999), we use different measured l_0
 260 values for each analyst.

261 The general form of g stems from the Box-Cox “super-model” used by Laslett et
 262 al. (1987),

$$263 \quad g = \{[(1 - r^\beta)/\beta]^\alpha - 1\}/\alpha \quad (2)$$

264 Certain values of α and β simplify the equation. Following from the final recommended
 265 model of Ketcham et al. (2007b), we use $\beta = -1$, and simplify further by folding the final
 266 terms into the C_i parameters for f .

267 To account for the possibility of a longer “true” initial track length, and to permit
 268 inclusion of short-time-scale measurements while still using a 2-12-month post-
 269 irradiation measurement for l_0 , we include an adjustment factor τ to modify l_0 , resulting
 270 in:

$$271 \quad g = \left(\frac{\tau}{r} - 1\right)^\alpha \quad (3)$$

272 The relation between τ , l_0 , and μ_{\max} is $\mu_{\max} = \tau l_0$. To ensure $\tau/r > 1$, the minimum value
 273 for τ is $1.0001 l_{\max}/l_0$, where l_{\max} is the maximum mean length measured (in each case
 274 here, the value at $3.66 \ln(s)$), and it is allowed to vary up to a maximum of 1.2, meaning
 275 the adjusted initial length is allowed to be up to 20% longer than the value measured
 276 months after irradiation.

277 We investigate two empirical models proposed previously to describe the
 278 annealing of fission tracks. The fanning Arrhenius model (FA) (Laslett et al., 1987),

$$279 \quad f = C_0 + C_1 \left[\frac{\ln(t) - C_2}{(1/T) - C_3} \right] \quad (4)$$

280 defines a single fanning point in Arrhenius space and fits a set of linear iso-annealing
 281 contours emanating from that point. The fanning curvilinear model (FC) (Crowley et al.,
 282 1991; Ketcham et al., 1999),

$$283 \quad f = C_0 + C_1 \left[\frac{\ln(t) - C_2}{\ln(1/T) - C_3} \right] \quad (5)$$

284 is similar but fits fanning contours that are linear in log-log space but slightly curved in
 285 Arrhenius space.

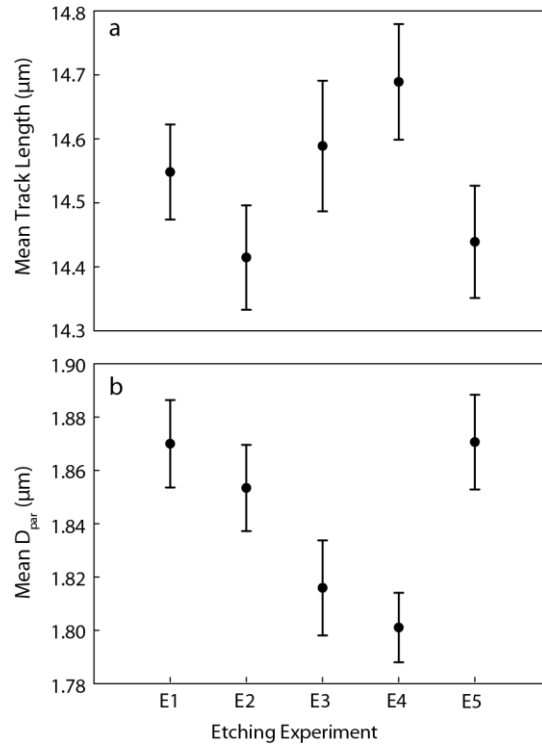
286 In keeping with previous work, we explore functions fit to both mean length and
 287 mean c-axis projected length data. Although we also calculated individual ellipse fits for
 288 all experiments, the results showed excess scatter, due largely to the sparsity of low-angle
 289 tracks (Donelick et al., 1999; Ketcham, 2003). We fitted the model parameters using chi-
 290 squared minimization as described by Ketcham et al. (1999, Appendix A). Results are
 291 accompanied by a series of index temperatures helpful for inferring geological time-scale
 292 predictions (Ketcham et al., 1999). The closure temperature (T_C) is the temperature of the
 293 measured age (Dodson 1973, 1986) assuming linear cooling from high temperature. The
 294 fading temperature (T_F) is the down-hole temperature where fission track density drops to
 295 zero after isothermal holding of a given duration (Gleadow & Duddy, 1981; Naeser et al.,
 296 1981). The total annealing temperature (T_A) defines where a fission-track population will
 297 totally anneal with linear heating, or equivalently the highest temperature experienced by
 298 any surviving fission track during cooling (Issler, 1996; Ketcham et al., 1999). T_C and T_A
 299 are given for various cooling rates (in °C/m.y.); and T_F varies with the duration of the
 300 isothermal episode (given in m.y).

301 **4 Results**

302 4.1 Durango spontaneous track monitor samples

303 The mean track length and etch figure measurements of the monitor samples are
 304 listed in Table 2, and shown in Figure 1. The monitor data show no systematic change,
 305 and variation is minor, with a range of $<0.3 \mu\text{m}$ for mean track length and $<0.1 \mu\text{m}$ for
 306 mean D_{par} value, verifying that etching procedures were consistent across the experiment,

307 and that the subtle length changes reported below are within the resolution limit of this
 308 study.



309
 310 **Figure 1:** Mean track length and D_{par} measurements of Durango apatites co-etched with
 311 each etching experiment.

312 4.2 Ambient-temperature annealing

313 Summaries of non-projected and **c**-axis projected track length measurements, as
 314 well as fitted ellipse axes, are listed in Table 3. The mean non-projected and projected
 315 track lengths from this study, combined with data from Tamer et al. (2019), Donelick et
 316 al. (1990), and Carlson et al. (1999) are shown as points with error bars in Figure 2. Also
 317 shown for reference are spontaneous track length measurements for each apatite,
 318 although they are non-equivalent to the experimental induced-track data in at least two
 319 ways. First, the individual tracks are of varying age, having formed continuously
 320 throughout the samples' respective geological histories; for this reason, we plot each
 321 point at half the sample age, to represent the mean age of the spontaneous tracks.
 322 Second, their annealing temperatures are unknown, although the assumption that the
 323 Durango and Fish Canyon localities remained near the Earth surface has independent
 324 support (Gleadow et al., 2015; McDowell et al., 2005).

325

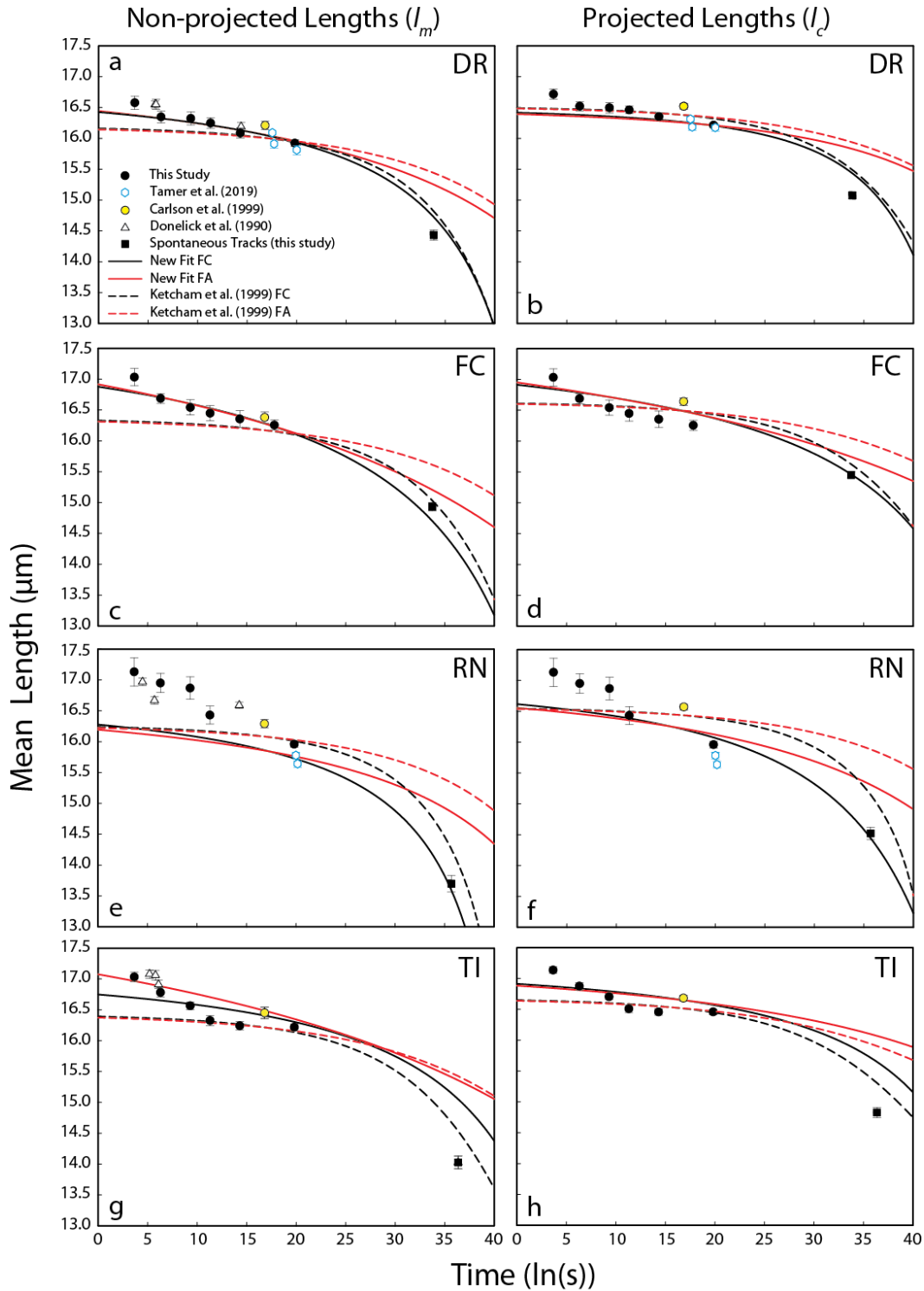
326 **Table 3.** *Non-projected, modeled c-axis projected, and ellipse fits to confined fission-*
 327 *track lengths.*

Apatite	Track age (ln(s))	<i>N</i>	<i>l_m</i> (μm)	σ_m	<i>l_{c,mod}</i> (μm)	$\sigma_{l_{c,mod}}$	<i>l_{c,fit}</i> (μm)	<i>l_{a,fit}</i> (μm)	σ_{ellipse}
DR	3.66	26	16.58 (11)	0.54	16.72 (09)	0.44	16.71 (51)	16.52 (25)	0.54
	7.00	29	16.35 (10)	0.54	16.52 (08)	0.43	16.24 (32)	16.40 (19)	0.54
	10.00	33	16.32 (11)	0.61	16.50 (09)	0.51	16.55 (27)	16.15 (22)	0.60
	12.00	33	16.25 (09)	0.49	16.46 (06)	0.36	16.47 (38)	16.16 (19)	0.49
	15.00	28	16.09 (09)	0.45	16.35 (07)	0.35	16.23 (48)	16.04 (19)	0.45
	18.32 ^{1,3}	169	16.06 (05)	0.68	16.32 (04)	0.51	16.31 (18)	15.96 (09)	0.67
	20.51	177	15.92 (05)	0.70	16.21 (04)	0.52	16.29 (16)	15.77 (08)	0.69
	20.56 ¹	158	15.90 (06)	0.74	16.20 (04)	0.56	16.02 (17)	15.86 (09)	0.74
	20.74 ¹	159	15.84 (06)	0.72	16.15 (04)	0.53	16.28 (17)	15.65 (09)	0.70
	34.53 ²	87	14.43 (08)	0.78	15.08 (06)	0.54	15.21 (20)	14.06 (12)	0.69
FC	3.66	28	17.03 (14)	0.73	17.12 (12)	0.66	17.33 (36)	16.99 (22)	0.72
	7.00	45	16.69 (08)	0.54	16.79 (07)	0.46	16.51 (30)	16.78 (19)	0.54
	10.00	26	16.54 (12)	0.63	16.67 (10)	0.53	16.66 (39)	16.47 (25)	0.63
	12.00	32	16.45 (12)	0.69	16.63 (10)	0.56	16.70 (43)	16.36 (20)	0.69
	15.00	23	16.35 (13)	0.64	16.52 (12)	0.56	16.14 (36)	16.50 (28)	0.64
	18.49 ³	57	16.26 (08)	0.62	16.47 (06)	0.47	16.78 (29)	16.02 (15)	0.59
	34.43 ²	109	14.93 (07)	0.71	15.45 (05)	0.56	15.09 (20)	14.86 (11)	0.71
	RN	3.66	9	17.13 (23)	0.69	17.19 (21)	0.64	17.57 (56)	16.92 (34)
7.00		10	16.95 (16)	0.50	17.01 (14)	0.44	16.10 (73)	17.04 (35)	0.49
10.00		9	16.87 (16)	0.55	16.93 (16)	0.49	16.56 (50)	17.09 (41)	0.52
12.00		14	16.43 (14)	0.54	16.59 (11)	0.43	15.84 (59)	16.68 (32)	0.50
15.00 ³		18	16.11 (12)	0.51	16.32 (10)	0.44	15.83 (43)	16.27 (28)	0.49
20.51		151	15.96 (05)	0.64	16.27 (04)	0.46	16.59 (26)	15.80 (08)	0.62
20.56 ¹		164	15.78 (06)	0.71	16.09 (04)	0.54	15.95 (16)	15.66 (09)	0.71
20.74 ¹		170	15.64 (06)	0.73	15.97 (04)	0.55	15.82 (14)	15.54 (09)	0.72
36.30 ²		106	13.70 (13)	1.39	14.52 (10)	1.04	14.35 (19)	13.39 (11)	1.36
TI	3.66	72	17.03 (08)	0.65	17.14 (07)	0.56	17.33 (22)	16.88 (13)	0.64
	7.00	66	16.78 (07)	0.60	16.87 (06)	0.52	16.82 (22)	16.76 (13)	0.60
	10.00	59	16.56 (07)	0.50	16.70 (05)	0.41	16.41 (30)	16.62 (15)	0.50
	12.00	50	16.33 (08)	0.58	16.51 (06)	0.45	16.43 (31)	16.27 (18)	0.58
	15.00	69	16.24 (07)	0.58	16.45 (05)	0.45	16.37 (27)	16.19 (14)	0.58
	20.51 ³	148	16.22 (06)	0.68	16.46 (04)	0.50	16.92 (21)	16.00 (08)	0.64
	37.05 ²	113	14.03 (10)	1.10	14.80(08)	0.83	14.45 (20)	13.87 (10)	1.09

328 ¹Measurement data from Tamer et al. (2019). ²Apatites with spontaneous tracks; AFT
 329 ages for DR, FC, RN; monazite U/Pb for TI. ³Experiment used for *l₀*.

330

331



332

333 **Figure 2:** Evolution of mean non-projected (a,c,e,g) and c-axis projected (b,d,f,h) track
 334 length with time at ambient temperatures, with new (solid) and previous (dashed) model
 335 fits for four apatites from four data sets. FA = fanning Arrhenius, FC = fanning
 336 curvilinear.

337 In all four apatites, for both projected and non-projected lengths, there is a continuous
338 decrease in mean track length with time at ambient temperatures. Broadly speaking, all four
339 show a pattern of initial fast annealing that slows down as time scales extend from seconds to
340 years. However, the timing and severity of this deceleration varies among apatites. DR and FC
341 annealing rates decelerate after the first experiment, while TI annealing appears to decelerate
342 after the fourth. RN apatite has an unusual pattern of apparent initial slow annealing followed by
343 acceleration and then deceleration, though the signal is unclear due to very low track numbers
344 stemming from its low U content. However, the longer-time-scale RN data ($\ln(s)=15-20$) imply a
345 continuing fast annealing trend not evident for the other apatites.

346 Our measurements are broadly consistent with prior work by Donelick et al. (1990). Data
347 for DR are extremely congruent, and the RN pattern is similar in its irregularity, especially
348 considering the Carlson et al. (1999) l_0 value by the same analyst (R. Donelick), though the
349 earlier measurement used a different etching protocol. Perhaps the largest difference is that the
350 Donelick et al. (1990) and Carlson et al. (1999) data for Tioga apatite seem to define a consistent
351 trend, albeit one defined by two clusters of closely spaced points, whereas our data suggest two
352 stages with differing annealing rates.

353 Also shown in Figure 2 as dashed lines are the predicted lengths at 23°C for annealing
354 models by Ketcham et al. (1999). The models shown for DR and RN are the versions fitted to
355 only the data for those respective apatites (Ketcham et al., 1999, Table 3). Because Carlson et al.
356 (1999) only conducted 13 experiments for TI and FC, for those apatites we plotted the
357 predictions of the multi-apatite models (Ketcham et al., 1999, Table 5), using the apatites'
358 respective apatite-apatite fitting parameters r_{mr0} and κ (Ketcham et al., 1999, Table 4). In each
359 case, because the l_0 measured after ~1 year of ambient annealing was used for the previous
360 models, the maximum possible model track length was substantially shorter than the shorter-time
361 experiments reported here, precluding them from reproducing our new data. It should be noted,
362 however, that the Ketcham et al. (1999) equations do predict some annealing over month-to-
363 decade time scales, which is why they under-predict the plotted Carlson et al. (1999) l_0 points
364 (yellow circles in Figure 2), instead asymptotically approaching these values as log time
365 approaches $-\infty$. Also noteworthy is that the Carlson et al. (1999) fanning curvilinear curves for
366 DR and FC come close to the spontaneous track measurements, illustrating how those models
367 broadly agree with the low-temperature annealing benchmarks proposed by Ketcham et al.
368 (1999). Moreover, they are also close to the spontaneous track measurements for RN and TI,
369 suggesting that these apatites have also experienced at most limited heating over their geological
370 histories.

371 4.3 Annealing models

372 Fitted parameters for the annealing models calculated for this study are shown in Table 4,
373 and the index temperatures showing their geological time-scale predictions are listed in Table 5.
374 The predicted annealing curves 23°C, representing a reasonable ambient temperature and
375 adopted by convention from Donelick et al. (1990), are shown as solid lines in Figure 2. When
376 considering these results, it is important to keep in mind that in addition to the low-temperature
377 data shown there are varying amounts of high-temperature data (Table 4) that also influence the
378 model fits and resulting 23°C predictions.

379 **Table 4:** Annealing models for individual apatites: Model parameters.

Apatite	N ¹	N ²	N ³	Length type	Fit	χ^2_v	C ₀	C ₁	C ₂	C ₃	α	τ
DR	69	60	9	l _m	FC	1.54	-50.338	1.0255	-74.676	-8.1210	-0.8513	1.0594
					FA	1.46	-15.647	5.5043E-4	-16.178	7.5363E-4	-0.8984	1.0883
				l _c	FC	2.41	-54.628	1.1041	-105.28	-8.7728	-0.4104	1.0124
					FA	2.35	-15.132	5.0251E-4	-22.370	5.1659E-4	-0.3078	1.0124
FC	18	12	6	l _m	FC	0.58	-36.836	0.7574	-82.003	-8.3300	-1.0000	1.1072
					FA	0.42	-8.9095	3.03E-4	-14.500	7.77E-4	-1.0000	1.1616
				l _c	FC	0.52	-33.741	0.6379	-55.420	-7.7011	-1.0000	1.0856
					FA	0.58	-10.380	3.0835E-4	-11.992	9.1584E-4	-1.0000	1.1297
RN	63	55	8	l _m	FC	1.96	-80.451	1.7499	-102.12	-8.8076	-1.0000	1.0615
					FA	1.78	-22.018	8.5189E-4	-21.0071	5.1746E-4	-1.0000	1.0789
				l _c	FC	3.25	-23.320	0.4641	-37.2881	-7.3530	-0.3737	1.0166
					FA	3.00	-12.102	4.1411E-4	-13.9906	8.2108E-4	-0.3074	1.0166
TI	17	11	6	l _m	FC	1.35	-999.99	19.579	-2982.846	-65.0608	-1.0000	1.0845
					FA	1.27	-8.1882	2.5042E-4	-21.3969	6.1799E-4	-1.0000	1.1740
				l _c	FC	1.22	-997.96	19.866	-2072.036	-47.9494	-1.0000	1.0576
					FA	1.21	-22.185	6.8590E-4	-38.4459	4.9387E-6	-1.0000	1.0830

380 ¹Total number of data sets. ²Number of high-T data sets from Carlson et al. (1999). ³Number of low-T data sets from Tamer et al.
381 (2019) and this study
382

383 **Table 5:** Annealing models for individual apatite: predicted index temperatures and lengths.

Apatite	Data Sets	Length Type	Fit	T _{F,100}	T _{F,30}	T _{F,10}	T _{C,1}	T _{C,10}	T _{C,100}	T _{A,1}	T _{A,10}	T _{A,100}	<i>r</i> _{Vrol,mean} ²	<i>r</i> _{FC}
DR	High-T ¹	l _m	FC	83.1	92.1	100.4	89.2	107.2	126.4	102.5	120.4	139.1	-	-
			FA	117.5	124.1	130.3	121.5	135.4	150.3	133.5	146.9	161.3	-	-
		l _c *	FC	96.9	106.0	114.5	94.4	112.5	131.8	116.5	134.6	153.6	-	-
			FA	131.0	137.8	144.1	126.0	140.0	154.9	147.2	161.0	175.6	-	-
	Combined	l _m	FC	88.1	97.0	105.3	92.6	110.5	129.7	107.4	125.2	143.8	-	-
			FA	121.8	128.3	134.5	123.5	137.3	152.2	137.7	151.1	165.3	-	-
		l _c	FC	97.2	106.3	114.9	94.2	112.4	131.7	116.8	135.1	154.2	-	-
			FA	132.1	138.8	145.2	126.0	140.0	155.0	148.3	162.1	176.9	-	-
FC	High-T ¹	l _m	FC	113.7	123.0	131.7	109.6	128.1	147.8	133.6	152.1	171.5	-	0.9134
			FA	148.3	155.2	161.7	142.0	156.3	171.7	164.7	178.8	193.7	-	0.9522
		l _c	FC	121.9	131.1	139.7	112.9	131.2	150.8	141.6	159.9	179.1	-	0.9389
			FA	155.4	162.3	168.7	144.5	158.7	174.0	171.8	185.7	200.6	-	0.9658
	Combined	l _m	FC	105.6	115.0	123.7	105.4	124.1	143.9	125.5	144.3	163.9	-	0.9171
			FA	143.0	149.8	156.3	138.2	152.5	167.9	159.4	173.4	188.3	-	0.9460
		l _c	FC	121.2	130.3	138.8	113.6	131.6	150.7	140.7	158.8	177.7	-	0.9441
			FA	156.9	163.6	169.9	144.5	158.4	173.4	173.0	186.6	201.0	-	0.9626
RN	High-T ¹	l _m	FC	70.4	79.2	87.4	76.6	94.0	112.6	89.6	107.1	125.5	0.9101	-
			FA	104.8	111.3	117.3	108.4	121.9	136.4	120.6	133.7	147.8	0.9517	-
		l _c *	FC	85.1	94.1	102.6	79.5	97.1	115.9	104.6	122.6	141.5	0.9280	-
			FA	117.6	124.2	130.5	110.4	124.1	138.8	133.7	147.3	161.9	0.9650	-
	Combined	l _m	FC	65.2	74.1	82.4	72.2	89.9	108.9	84.5	102.4	121.2	0.8922	-
			FA	100.9	107.5	113.6	104.8	118.4	133.2	116.8	130.2	144.5	0.9433	-
		l _c	FC	88.2	97.1	105.3	81.3	98.5	117.0	107.4	125.0	143.5	0.9197	-
			FA	119.8	126.3	132.5	111.3	124.9	139.5	135.7	149.1	163.4	0.9596	-
TI	High-T ¹	l _m	FC	154.6	164.4	173.4	132.1	151.1	171.2	175.0	194.4	214.6	-	-
			FA	189.8	197.0	203.9	164.7	179.4	195.1	206.8	221.5	237.2	-	-
		l _c	FC	196.9	206.7	215.8	145.9	164.6	184.6	217.3	236.7	256.8	-	-
			FA	233.1	240.5	247.4	177.8	192.5	208.2	250.3	265.1	280.9	-	-
	Combined	l _m	FC	124.3	133.7	142.6	124.5	143.2	162.9	144.4	163.3	183.0	-	-
			FA	167.3	174.2	180.6	159.0	173.1	188.2	183.7	197.7	212.5	-	-
		l _c	FC	125.9	135.6	144.6	121.7	140.5	160.4	146.3	165.6	185.8	-	-
			FA	161.6	168.8	175.5	153.3	167.7	183.2	178.5	193.1	208.6	-	-

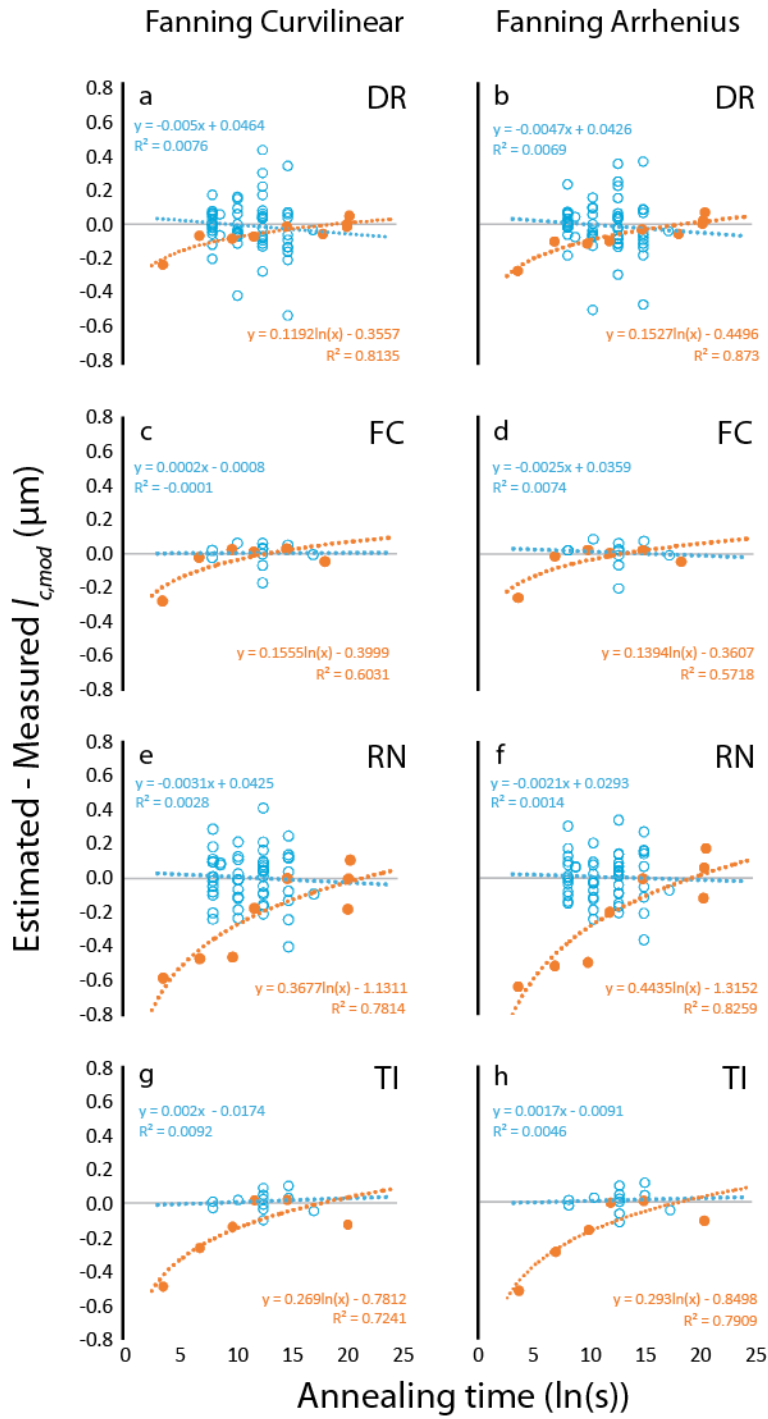
384 ¹ High-T index temperatures from Ketcham et al. (1999), except asterisks indicate index temperatures from Ketcham et al. (2007). ² Reduced
385 length for fluorapatite based on Vrolijk et al. (1992); target values 0.890-0.925 (non-projected), 0.925-0.950 (c-axis projected). ³ Reduced length
386 for FC apatite based on Ketcham et al. (2007); target values 0.937 ± 0.006 (non-projected), 0.959 ± 0.005 (c-axis projected).

387 The new models display a range of behaviors in comparison to the Ketcham et al. (1999)
388 models. For DR apatite (Fig. 2a, b), the new model fits all of the low-temperature data well, with
389 the exception of the shortest-time experiment. The fanning curvilinear fit also closely matches
390 the spontaneous data, while the closure temperatures (Table 5) are only changed by 2-3°C, and
391 other index temperatures by 4-7°C. Results are similarly congruent for FC apatite (Fig. 2c, d).
392 Divergences are somewhat greater for the fanning Arrhenius models, and for the l_m versus the l_c
393 models. These results suggest that the empirical fanning curvilinear fit to **c**-axis projected data is
394 able to incorporate low-temperature, short-time data well, with a suitable change in the
395 normalizing value. However, the normalizing values themselves show considerable variation,
396 from 2.5% to 19.7% above the one-year-annealing l_0 measurements.

397 In contrast, the RN apatite models struggle to encompass the low-T data. This is in part
398 due to the constraints imposed by the numerous high-temperature data, but it is also clear that
399 neither model form or data type can encompass the low-T trend. Similarly, the TI models cannot
400 fit the apparent two-component trend in our data, although, interestingly, they are consistent
401 with, though offset from, the Donelick et al. (1990) data. In terms of index temperatures (Table
402 5), adding in the RN low-T data changes the results slightly more than for DR, although
403 predicted closure temperatures still agree to within 4°C. The mismatch in TI index temperatures
404 is greater, in part because the Ketcham et al. (1999) high-T models were fit in concert with all
405 other apatites in Carlson et al. (1999), whereas here only TI data are being fitted. In particular,
406 because the Carlson et al. (1999) TI data set includes no samples annealed to below a mean track
407 length of 11.8 μm , the near-total-annealing behavior of this apatite is not well constrained.

408 Figure 3 shows the time residuals of mean **c**-axis projected length for each of the new
409 models, distinguishing between high-temperature and low-temperature data. Standardized
410 residuals (i.e. divided by uncertainty) are provided in the supplement and tell essentially the
411 same story. Residuals from both linear and curvilinear models for the high-temperature data are
412 flat to shallowly dipping; extending the linear fits to these residuals to geological time scales
413 ($\sim 35 \ln(\text{s})$) implies departures of 0.2 μm or less. Linear correlation coefficients are all less than
414 0.01. The larger DR and RN data sets show more scatter, but there is no readily apparent
415 structure to any of the residuals. The low-T data, however, show significant structure, and in
416 most cases are better fit by a logarithmic function than a line. The logarithmic fits imply a small
417 positive residual of $\sim 0.25 \mu\text{m}$ or less by 35 $\ln(\text{s})$ for the four apatites.

418



419

420

421 **Figure 3:** Time residuals of fitted model predictions for mean **c**-axis projected lengths for each
 422 apatite.

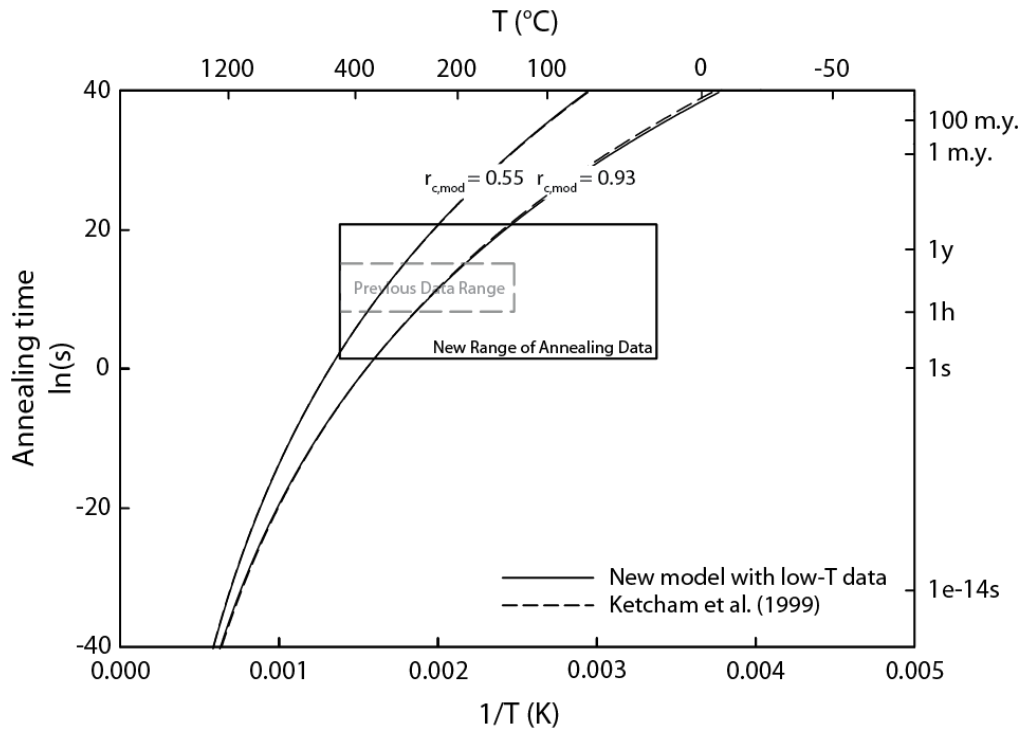
423 **5 Discussion**

424 5.1 Extending the range of annealing conditions

425 Apatite fission-track thermal history modelling is based on the extrapolation of annealing
426 of induced tracks at laboratory conditions to geological time scales. Typically, model parameters
427 are fitted by minimizing the misfit between model equation predictions and the data, and
428 different model equations are evaluated and compared based on their degree of misfit and
429 residuals (e.g., Laslett & Galbraith, 1996; Laslett et al., 1987), as well as their predictions against
430 geological benchmarks (Ketcham et al., 1999). Because the various proposed empirical
431 annealing equations overlap greatly over the limited time and temperature range of laboratory
432 experiments (e.g., Ketcham, 2019, Fig. 3.9), extending this range provides a new opportunity to
433 distinguish models by providing more space for them to diverge. Previous annealing studies
434 covered temperature ranges of ~100°C to ~450°C and durations from ~30 minutes up to a couple
435 of months, while this study extends annealing temperatures down to ~23°C and broadens the
436 time range to span from 39 seconds to ~32 years (Figure 4).

437 In terms of goodness of fit, Ketcham et al. (1999) found that the fanning Arrhenius
438 equation fit the Carlson et al. (1999) data slightly better than fanning curvilinear form, while
439 Ketcham et al. (2007b) found that data from Barbarand et al. (2003) was sometimes better fit
440 using the fanning curvilinear equation, depending on the form of g used. In this study (Table 4),
441 we find that combined low-T and high-T DR and RN experimental data from Carlson et al.
442 (1999) and this study were slightly better fit by the fanning Arrhenius form, while the TI and FC
443 data were somewhat more closely fitted by the fanning curvilinear equation. Given that the DR
444 and RN data sets show more extreme scatter (Fig. 3) and that χ^2_v values are most sensitive to the
445 most scattered points, we infer that the laboratory-time-scale data alone do not provide clear
446 evidence of the superiority of one model form over the other, and that other considerations such
447 as geological comparisons remain more informative.

448 While there is no discernible structure in the high-temperature residuals, the low-
449 temperature data show a clear structure that diminishes with time. This suggests that there is a
450 process occurring in the immediate aftermath of track formation that is not captured by either
451 empirical annealing equation, but that this process may have a limited impact at longer
452 laboratory or geological time scales.



453

454 **Figure 4:** Illustration of extended range laboratory annealing data, and comparison of
 455 extrapolated predictions at low ($r_{c,mod} = 0.93$) and high ($r_{c,mod} = 0.55$) annealing conditions.

456 5.2 Geological predictions

457 Our fanning curvilinear fits for the DR and FC apatites both reproduce earlier work
 458 (Ketcham et al., 2007b; Ketcham et al., 1999) in making predictions that reasonably match their
 459 respective spontaneous track length data (Fig. 2a,b). As Figure 4 illustrates, the contours
 460 corresponding to reduced c-axis-projected length values for geological low-temperature (0.93)
 461 and total (0.55) annealing are not significantly impacted by incorporating the new data or making
 462 the true initial track length a fitted value. It is thus clear that incorporating the new low-
 463 temperature data did nothing to harm the geological predictions of these models based on
 464 apatites at both localities having resided at near-earth-surface temperatures since formation.

465 We also provide the first similar evaluation of Renfrew and Tioga apatites. Although the
 466 long-term burial histories at each locality are not known, both are likely to reflect long-term low-
 467 temperature histories. Renfrew, Ontario, is on the Canadian Shield, in an area of long-term
 468 stability. The apatite fission-track reference age for this locality is 184 ± 15 Ma (Van Den Haute
 469 & Chambaudet, 1990), while the U-Pb age of the enclosing pegmatite is ~ 1 Ga (Larsen et al.,
 470 1952). The Tioga apatite locality, near Old Port, Pennsylvania, is in the midst of the Valley and
 471 Ridge province. It is enclosed within the Marcellus Shale, and monazites in Tioga material
 472 collected nearby give a U-Pb age of 390 Ma (Roden et al., 1990). Tioga apatite from our
 473 sample's locality has a (U-Th)/He age of 280 Ma (Shuster et al., 2006), supporting long
 474 residence time at temperatures that probably remained below 60°C . While this area has
 475 undergone a complex history involving some burial, Tioga apatite has a substantially higher than
 476 normal resistance to annealing, and thus a greater ability to retain long track lengths with minor
 477 heating.

478 Our Renfrew fanning curvilinear model closely replicates our spontaneous track data
479 assuming a mean track age of 92 Ma while residing at ~23°C. Our Tioga model predicts a
480 slightly higher track length than observed assuming a mean age of 195 Ma at ~23°C, but if the
481 residence temperature is raised to ~42°C the 15- μ m mean c-axis-projected length is matched.
482 These results, while rough and schematic, further support the idea that the fanning curvilinear
483 model makes reasonable predictions of fission-track annealing in the near-surface environment.
484 This in turn supports the validity of thermal history modeling results in the near-surface regime
485 that utilize apatite fission-track length data.

486 5.3 Possibility of annealing due to secondary radiation

487 Our data strongly imply a second annealing mechanism in the initial stages, with different
488 controlling equations or parameters. In particular, all four apatites show observable annealing in
489 excess of the empirical model fits between the 39-second and 18-minute etching steps. A natural
490 mechanism to consider is the secondary radiation produced by short-lived isotopes created
491 during the irradiation. Other than induced fission of ^{235}U , several isotopes found in apatite in
492 potentially significant quantities (^{19}F , ^{23}Na , ^{31}P , ^{35}Cl , $^{40,44}\text{Ca}$, ^{55}Mn , ^{88}Sr , ^{139}La , ^{140}Ce ,
493 $^{146,148,150}\text{Nd}$) interact with thermal neutrons through n, α and n, γ reactions to produce radioactive
494 isotopes. Table S1 lists the unstable daughter products and their decay modes and half-lives,
495 which range from seconds to months. The table also shows the estimated vacancies per decay
496 caused by recoil, estimated using SRIM-2013 (Ziegler, 2013). We presume that only recoil
497 damage is likely to affect track stability, and that emitted electrons and photons are not
498 important; no significant activation products in apatite produce alpha particles. The only beta
499 particle energetic enough to incur a recoil that results in any vacancies at all is ^{20}F produced from
500 ^{19}F , and it averages 0.44 vacancies created per ion and has a stopping distance averaging 0.71
501 nm.

502 To scale the volume density of secondary recoils and the resulting damage to the fission
503 damage zone, we normalize the density of decays and vacancies generated in Durango apatite at
504 each stage of our experiment to the volume encompassed by a fission track. We estimate the
505 latter as an ellipsoid with two short radii of 4.5 nm (Li et al., 2010) and one long radius of 9 μ m.
506 As of the end of the first etching step (39s), we find that there remain 6.2×10^{-5} activated ^{20}F
507 atoms per track volume, which will have decayed by the second etching step, generating $2.75 \times$
508 10^{-5} vacancies per track volume. From these results, it is evident that recoil damage from
509 activated isotopes is insufficient to have any effect on annealing rates.

510 5.4 Seasoning

511 Another candidate annealing mechanism is “seasoning,” a vaguely defined process
512 posited by several authors to explain track shortening at low temperatures (e.g., Durrani & Bull,
513 1987), possibly accompanied by a lack of apparent age reduction (Wauschkuhn et al., 2015).
514 More generally, it can also serve as a placeholder for spontaneous tracks behaving differently
515 from induced ones. Could the low-temperature annealing observed here correspond to seasoning,
516 or at least one aspect of it?

517 At this stage, it is difficult to answer this question. Given that the effect we observe
518 occurs at very short time scales, and seems to fade to insignificance at month-to-year time scales,
519 much less millions-of-year ones, how it might apply to geological observations is unclear. One
520 possibility is that it may be already broadly incorporated into the empirical fanning curvilinear

521 annealing equation. The curvature in the predicted annealing contours essentially posit more
522 geological-time-scale annealing than the fanning linear forms that more closely reflect standard
523 kinetics based on the Arrhenius equation. This curvature may be ascribable to temperature
524 dependence in the kinetic frequency factor (Carlson, 1990; Ketcham, 2019), but superposition of
525 multiple mechanisms may be a reasonable alternative. For example, molecular dynamics
526 modeling suggests that there are multiple damage types and states within a track, ranging from
527 slightly distorted lattice to amorphous or glassy material (Rabone et al., 2008), and different
528 components of damage may anneal at different rates or by different mechanisms. Such variation
529 may also underlie the different etching characteristics of spontaneous and induced fission tracks
530 (Jonckheere et al., 2017).

531 A corollary question, posed in the title of this paper, is whether low-temperature
532 annealing is a thermally controlled process. Certainly, insofar as much of our month-to-decade
533 and geological data appear to be well described by the empirical equations, it is evident that most
534 low-temperature annealing is indeed thermally controlled. However, with regard to an early-
535 stage fast annealing process, our data are not sufficient to discern, if only because they only
536 involve a single temperature; similar data at different temperatures may help address this
537 question and elucidate details of the mechanism at work.

538 Yet another applicable question is how apatite composition may affect an early, low-
539 temperature annealing process. The magnitude and rate of low-T annealing shows a fair degree
540 of variation. In three of our four apatites (DR, FC, TI), annealing pathways essentially converge
541 with the fanning curvilinear model within a month, while RN apatite is arguably still undergoing
542 low-temperature annealing after 30 years, with double the net magnitude. The next most severe
543 instance in terms of timing and departure from the fanning curvilinear model is TI. We are
544 unable, however, to distinguish what features of these apatites may set them apart from the
545 others. In both cation and anion compositions, RN and TI are the extremes of our apatites in
546 terms of chemistry, and bracket DR and FC (Table 2). More data would thus be required to
547 determine what features might influence the early, low-temperature process.

548 5.5 Reconsideration of mean unannealed track length

549 The data of our study indicate that mean “unannealed” track lengths decrease over
550 seconds to years, with measured decreases of 0.74 μm for DR, 0.77 μm for FC, 1.49 μm for RN,
551 and 0.81 μm for TI, with the majority of annealing occurring within the first month after
552 irradiation. The cool-down waiting period after thermal neutron irradiation thus has a direct
553 effect on the measured l_0 , as well as any subsequent waiting time. Moreover, it is likely that the
554 annealing of a fission track starts from the moment of its registration in the crystal lattice until it
555 is etched. It is impossible to register and etch a fission track instantly and simultaneously, and
556 therefore any track we observe is annealed to some degree.

557 Laslett and Galbraith (1996) proposed that the “true” unannealed length (μ_{max}), or at least
558 the most appropriate value for normalizing measurements of annealed tracks, might be obtained
559 by allowing it to be a free parameter when fitting an annealing model. However, their results,
560 those of Ketcham et al. (2007b; 1999), and the results in this study suggest that this approach is
561 not productive. Not only do the posited initial track lengths (μ_{max} or τl_0) vary much more widely
562 than is reasonably suggested by the data themselves, but the possibility of an additional
563 annealing mechanism responsible for the earliest stages of length reduction further muddies the
564 picture. If the early-stage low-temperature annealing is not expressed in the high-temperature

565 annealing data, then using the high-temperature data to see back through early annealing cannot
566 work.

567 At the same time, initial track length is important for incorporating differences both
568 among apatites (Carlson et al., 1999) and among analysts (Ketcham et al., 2015; Ketcham et al.,
569 2009; Ketcham et al., 2018) into the thermal history inverse modeling process. To the extent that
570 thermal history results should be robust and reproducible, some method of normalization is
571 required.

572 Based on our understanding of our results, we suggest that, when characterizing an
573 unknown apatite, waiting through the fastest-declining part of the early annealing period is the
574 safest method to measure an initial track length that will be consistent with literature values, and
575 thus for comparison and usage across laboratories. Time after irradiation should be included
576 when results are reported. Interested research groups may wish to make multiple grain mounts
577 etched at various times after irradiation, to test or extend our results. Standardizing
578 measurements to a particular time after irradiation may eventually be worthwhile, but because
579 the low-temperature annealing process is poorly understood and likely of low magnitude after
580 the first month, we do not yet consider such measures to be warranted.

581 **6 Conclusions**

582 Mean induced fission track lengths in apatite decrease from as early as 39 seconds after
583 irradiation up to 32 years at room temperatures, with declines ranging from 0.7 to 1.5 μm . The
584 rate of decrease can be separated into two behaviors, with faster shortening at early stages and
585 slower shortening over longer periods at ambient temperatures that merges with trends predicted
586 from empirical annealing equations. We thus posit the earlier behavior to reflect a mechanism
587 not encompassed by the empirical equations. Although the rate, duration and magnitude of early-
588 stage low-temperature annealing vary among the apatites we studied, we could not discern what
589 chemical factors may control or influence this process. Fitted annealing models that combine
590 high-T and low-T annealing better encompassed the low-T data but made similar geological
591 time-scale predictions to models based on high-T data only. Comparison with spontaneous track
592 data corroborates previous results indicating that the fanning curvilinear model form reasonably
593 encompasses annealing at earth-surface temperatures. Additional experiments with more apatite
594 varieties and/or at different temperatures may help us to discern more concerning the earlier
595 annealing mechanism and further improve our knowledge of the annealing process.

596

597 **Acknowledgments, Samples, and Data**

598 This research was supported by the Jackson School of Geosciences at the University of Texas at
599 Austin. It was also supported in part by National Science Foundation grant EAR-0948636 to
600 RAK. We particularly thank Tracy Tipping of the Nuclear and Radiation Engineering Program
601 and laboratory manager at the Nuclear Engineering Teaching Laboratory at the University of
602 Texas at Austin for his help in planning and arranging for the experiment. We thank A. Gleadow
603 for providing Renfrew apatite material for this study. We thank A. Gleadow, R. Jonckheere, and
604 M. Cloos for helpful comments on an earlier version of this text. There are no financial conflicts
605 of interest for either author. All measurements are available from the Texas Data Repository
606 (<https://doi.org/10.18738/T8/CUA8F8>).

607

608 **References**

609

610

- 611 Barbarand, J., Carter, A., Wood, I., & Hurford, A. J. (2003). Compositional and structural control of fission-track
 612 annealing in apatite. *Chemical Geology*, 198, 107-137. [https://doi.org/10.1016/S0009-2541\(02\)00424-2](https://doi.org/10.1016/S0009-2541(02)00424-2)
- 613 Belton, D. X. (2006). *The low-temperature thermochronology of cratonic terranes*. (PhD), University of Melbourne,
 614 Retrieved from hdl.handle.net/11343/38119
- 615 Carlson, W. D. (1990). Mechanisms and kinetics of apatite fission-track annealing. *American Mineralogist*, 75,
 616 1120-1139.
- 617 Carlson, W. D., Donelick, R. A., & Ketcham, R. A. (1999). Variability of apatite fission-track annealing kinetics I:
 618 Experimental results. *American Mineralogist*, 84, 1213-1223. <https://doi.org/10.2138/am-1999-0901>
- 619 Crowley, K. D., Cameron, M., & Schaefer, R. L. (1991). Experimental studies of annealing etched fission tracks in
 620 fluorapatite. *Geochimica et Cosmochimica Acta*, 55, 1449-1465. [https://doi.org/10.1016/0016-](https://doi.org/10.1016/0016-7037(91)90320-5)
 621 [7037\(91\)90320-5](https://doi.org/10.1016/0016-7037(91)90320-5)
- 622 Donelick, R. A. (1991). Crystallographic orientation dependence of mean etchable fission track length in apatite: An
 623 empirical model and experimental observations. *American Mineralogist*, 76(1-2), 83-91.
- 624 Donelick, R. A., Ketcham, R. A., & Carlson, W. D. (1999). Variability of apatite fission-track annealing kinetics II:
 625 Crystallographic orientation effects. *American Mineralogist*, 84, 1224-1234. [https://doi.org/10.2138/am-](https://doi.org/10.2138/am-1999-0902)
 626 [1999-0902](https://doi.org/10.2138/am-1999-0902)
- 627 Donelick, R. A., & Miller, D. S. (1991). Enhanced TINT fission track densities in low spontaneous track density
 628 apatites using ²⁵²Cf-derived fission fragment tracks: A model and experimental observations. *Nuclear*
 629 *Tracks and Radiation Measurements*, 18(3), 301-307. [https://doi.org/10.1016/1359-0189\(91\)90022-A](https://doi.org/10.1016/1359-0189(91)90022-A)
- 630 Donelick, R. A., O'Sullivan, P. B., & Ketcham, R. A. (2005). Apatite fission-track analysis. In P. W. Reiners & T.
 631 A. Ehlers (Eds.), *Low-Temperature Thermochronology* (Vol. 58, pp. 49-94). Chantilly, VA: Mineralogical
 632 Society of America. <https://doi.org/10.2138/rmg.2005.58.3>
- 633 Donelick, R. A., Roden, M. K., Mooers, J. D., Carpenter, B. S., & Miller, D. S. (1990). Etchable length reduction of
 634 induced fission tracks in apatite at room temperature (~23°C): Crystallographic orientation effects and
 635 "initial" mean lengths. *Nuclear Tracks and Radiation Measurements*, 17(3), 261-265.
 636 [https://doi.org/10.1016/1359-0189\(90\)90044-X](https://doi.org/10.1016/1359-0189(90)90044-X)
- 637 Durrani, S. A., & Bull, R. K. (1987). *Solid State Nuclear Track Detection* (Vol. 111). Oxford: Pergamon.
- 638 Fleischer, R. L., & Price, P. B. (1964). Techniques for geological dating of minerals by chemical etching of fission
 639 fragment tracks. *Geochimica et Cosmochimica Acta*, 28(10-11), 1705-1714. [https://doi.org/10.1016/0016-](https://doi.org/10.1016/0016-7037(64)90017-1)
 640 [7037\(64\)90017-1](https://doi.org/10.1016/0016-7037(64)90017-1)
- 641 Fleischer, R. L., Price, P. B., & Walker, J. D. (1965a). Effects of temperature, pressure, and ionization of the
 642 formation and stability of fission tracks in minerals and glasses. *Journal of Geophysical Research*, 70(6),
 643 1497-1502. <https://doi.org/10.1029/JZ070i006p01497>
- 644 Fleischer, R. L., Price, P. B., & Walker, R. M. (1965b). Tracks of charged particles in solids. *Science*, 149(3682),
 645 383-393. <https://www.jstor.org/stable/1716484>
- 646 Fleischer, R. L., Price, P. B., Walker, R. M., & Maurette, M. (1967). Origins of fossil charged-particle tracks in
 647 meteorites. *Journal of Geophysical Research*, 72(1), 331-353. <https://doi.org/10.1029/JZ072i001p00331>
- 648 Gleadow, A. J. W., & Duddy, I. R. (1981). A natural long-term track annealing experiment for apatite. *Nuclear*
 649 *Tracks and Radiation Measurements*, 5, 169-174. [https://doi.org/10.1016/0191-278X\(81\)90039-1](https://doi.org/10.1016/0191-278X(81)90039-1)
- 650 Gleadow, A. J. W., Duddy, I. R., Green, P. F., & Lovering, J. F. (1986). Confined fission track lengths in apatite: a
 651 diagnostic tool for thermal history analysis. *Contributions to Mineralogy and Petrology*, 94, 405-415.
 652 <https://doi.org/10.1007/BF00376334>
- 653 Gleadow, A. J. W., Harrison, T. M., Kohn, B. L., Lugo-Zazueta, R., & Phillips, D. (2015). The Fish Canyon Tuff: A
 654 new look at an old low-temperature thermochronology standard. *Earth and Planetary Science Letters*, 424,
 655 95-108. <https://doi.org/10.1016/j.epsl.2015.05.003>
- 656 Green, P. F. (1988). The relationship between track shortening and fission track age reduction in apatite: Combined
 657 influences of inherent instability, annealing anisotropy, length bias and system calibration. *Earth and*
 658 *Planetary Science Letters*, 89, 335-352. [https://doi.org/10.1016/0012-821X\(88\)90121-5](https://doi.org/10.1016/0012-821X(88)90121-5)
- 659 Issler, D. R. (1996). Optimizing time step size for apatite fission track annealing models. *Computers and*
 660 *Geosciences*, 22, 67-74. [https://doi.org/10.1016/0098-3004\(95\)00057-7](https://doi.org/10.1016/0098-3004(95)00057-7)

- 661 Jonckheere, R. (2003). On methodical problems in estimating geological temperature and time from measurements
662 of fission tracks in apatite. *Radiation Measurements*, 36, 43-55. [https://doi.org/10.1016/S1350-](https://doi.org/10.1016/S1350-4487(03)00096-9)
663 [4487\(03\)00096-9](https://doi.org/10.1016/S1350-4487(03)00096-9)
- 664 Jonckheere, R., Tamer, M. T., Wauschkuhn, B., Wauschkuhn, F., & Ratschbacher, L. (2017). Single-track length
665 measurements of step-etched fission tracks in Durango apatite: “Vorsprung durch Technik”. *American*
666 *Mineralogist*, 102(5). <https://doi.org/10.2138/am-2017-5988>
- 667 Ketcham, R. A. (2003). Observations on the relationship between crystallographic orientation and biasing in apatite
668 fission-track measurements. *American Mineralogist*, 88, 817-829. <https://doi.org/10.2138/am-2003-5-610>
- 669 Ketcham, R. A. (2019). Fission-track annealing: From geologic observations to thermal history modeling. In M. G.
670 Malusà & P. G. Fitzgerald (Eds.), *Fission-Track Thermochronology and its Application to Geology*. Cham:
671 Springer. https://doi.org/10.1007/978-3-319-89421-8_3
- 672 Ketcham, R. A., Carter, A., & Hurford, A. J. (2015). Inter-laboratory comparison of fission track confined length
673 and etch figure measurements in apatite. *American Mineralogist*, 100, 1452-1468.
674 <https://doi.org/10.2138/am-2015-5167>
- 675 Ketcham, R. A., Carter, A. C., Donelick, R. A., Barbarand, J., & Hurford, A. J. (2007a). Improved measurement of
676 fission-track annealing in apatite using c-axis projection. *American Mineralogist*, 92, 789-798.
677 <https://doi.org/10.2138/am.2007.2280>
- 678 Ketcham, R. A., Carter, A. C., Donelick, R. A., Barbarand, J., & Hurford, A. J. (2007b). Improved modeling of
679 fission-track annealing in apatite. *American Mineralogist*, 92, 799-810.
680 <https://doi.org/10.2138/am.2007.2281>
- 681 Ketcham, R. A., Donelick, R. A., Balestrieri, M. L., & Zattin, M. (2009). Reproducibility of apatite fission-track
682 length data and thermal history reconstruction. *Earth and Planetary Science Letters*, 284, 504-515.
683 <https://doi.org/10.1016/j.epsl.2009.05.015>
- 684 Ketcham, R. A., Donelick, R. A., & Carlson, W. D. (1999). Variability of apatite fission-track annealing kinetics III:
685 Extrapolation to geological time scales. *American Mineralogist*, 84, 1235-1255.
686 <https://doi.org/10.2138/am-1999-0903>
- 687 Ketcham, R. A., Van Der Beek, P. A., Barbarand, J., Bernet, M., & Gautheron, C. (2018). Reproducibility of
688 thermal history reconstruction from apatite fission-track and (U-Th)/He data. *Geochemistry, Geophysics,*
689 *Geosystems*, 19. <https://doi.org/10.1029/2018GC007555>
- 690 Larsen, E. S. J., Keevil, N. B., & Harrison, H. C. (1952). Method for determining the age of igneous rocks using the
691 accessory minerals. *Geological Society of America Bulletin*, 63, 1046-1052. [https://doi.org/10.1130/0016-](https://doi.org/10.1130/0016-7606(1952)63[1045:MFDTAO]2.0.CO;2)
692 [7606\(1952\)63\[1045:MFDTAO\]2.0.CO;2](https://doi.org/10.1130/0016-7606(1952)63[1045:MFDTAO]2.0.CO;2)
- 693 Laslett, G. M., & Galbraith, R. F. (1996). Statistical modelling of thermal annealing of fission tracks in apatite.
694 *Geochimica et Cosmochimica Acta*, 60, 5117-5131. [https://doi.org/10.1016/S0016-7037\(96\)00307-9](https://doi.org/10.1016/S0016-7037(96)00307-9)
- 695 Laslett, G. M., Green, P. F., Duddy, I. R., & Gleadow, A. J. W. (1987). Thermal annealing of fission tracks in
696 apatite 2. A quantitative analysis. *Chemical Geology (Isotope Geoscience Section)*, 65, 1-13.
697 [https://doi.org/10.1016/0168-9622\(87\)90057-1](https://doi.org/10.1016/0168-9622(87)90057-1)
- 698 Li, N., Wang, L., Sun, K., Lang, M., Trautmann, C., & Ewing, R. C. (2010). Porous fission fragment tracks in
699 fluorapatite. *Physical Review B*, 82, 144109. <https://doi.org/10.1103/PhysRevB.82.144109>
- 700 McDowell, F. W., McIntosh, W. C., & Farley, K. A. (2005). A precise ⁴⁰Ar-³⁹Ar reference age for Durango apatite
701 (U-Th)/He and fission-track dating standard. *Chemical Geology*, 214, 249-263.
702 <https://doi.org/10.1016/j.chemgeo.2004.10.002>
- 703 Meitner, L., & Frisch, O. R. (1939). Disintegration of uranium by neutrons: a new type of nuclear reaction. *Nature*,
704 143(3615), 239-240. <https://doi.org/10.1038/143239a0>
- 705 Naeser, C. W. (1967). The use of apatite and sphene for fission track age determinations. *Geological Society of*
706 *America Bulletin*, 78(12), 1523-1526. [https://doi.org/10.1130/0016-](https://doi.org/10.1130/0016-7606(1967)78[1523:TUOAAAS]2.0.CO;2)
707 [7606\(1967\)78\[1523:TUOAAAS\]2.0.CO;2](https://doi.org/10.1130/0016-7606(1967)78[1523:TUOAAAS]2.0.CO;2)
- 708 Naeser, C. W., Zimmerman, R. A., & Cebula, G. T. (1981). Fission-track dating of apatite and zircon: An
709 interlaboratory comparison. *Nuclear Tracks and Radiation Measurements*, 5, 56-72.
710 [https://doi.org/10.1016/0191-278X\(81\)90027-5](https://doi.org/10.1016/0191-278X(81)90027-5)
- 711 Price, P. B., & Walker, R. M. (1963). Fossil tracks of charged particles in mica and the age of minerals. *Journal of*
712 *Geophysical Research*, 68(16), 4847-4862. <https://doi.org/10.1029/JZ068i016p04847>
- 713 Rabone, J. A. L., Carter, A., Hurford, A. J., & De Leeuw, N. H. (2008). Modelling the formation of fission tracks in
714 apatite minerals using molecular dynamics simulations. *Physics and Chemistry of Minerals*, 35, 583-596.
715 <https://doi.org/10.1007/s00269-008-0250-6>

- 716 Roden, M. K., Parrish, R. R., & Miller, D. S. (1990). The absolute age of the Eifelian Tioga ash bed, Pennsylvania.
717 *Journal of Geology*, 98(2), 282-285. www.jstor.org/stable/30063775 <https://doi.org/10.1086/629399>
- 718 Shuster, D. L., Flowers, R. M., & Farley, K. A. (2006). The influence of natural radiation damage on helium
719 diffusion kinetics in apatite. *Earth and Planetary Science Letters*, 249, 148-161.
720 <https://doi.org/10.1016/j.epsl.2006.07.028>
- 721 Silk, E. C. H., & Barnes, R. S. (1959). Examination of fission fragment tracks with an electron microscope.
722 *Philosophical Magazine*, 4(44), 970-972. <https://doi.org/10.1080/14786435908238273>
- 723 Spiegel, C., Kohn, B. L., Raza, A., Rainer, T., & Gleadow, A. J. W. (2007). The effect of long-term low-temperature
724 exposure on apatite fission track stability: A natural annealing experiment in the deep ocean. *Geochimica et*
725 *Cosmochimica Acta*, 71, 4512-4537. <https://doi.org/10.1016/j.gca.2007.06.060>
- 726 Tamer, M. T., Chung, L., Ketcham, R. A., & Gleadow, A. J. W. (2019). Analyst and etching protocol effects on the
727 reproducibility of apatite confined fission-track length measurement, and ambient-temperature annealing at
728 decadal timescales. *American Mineralogist*, 104, 1421-1435. <https://doi.org/10.2138/am-2019-7046>
- 729 Van Den Haute, P., & Chambaudet, A. (1990). Results of an interlaboratory experiment for the 1988 fission track
730 workshop on a putative apatite standard for internal calibration. *International journal of radiation*
731 *applications and instrumentation. Part D, Nuclear tracks and radiation measurements*, 17(3), 247-252.
732 [https://doi.org/10.1016/1359-0189\(90\)90042-V](https://doi.org/10.1016/1359-0189(90)90042-V)
- 733 Vrolijk, P., Donelick, R. A., Queng, J., & Cloos, M. (1992). Testing models of fission track annealing in apatite in a
734 simple thermal setting: site 800, leg 129. In R. L. Larson & Y. Lancelot (Eds.), *Proceedings of the Ocean*
735 *Drilling Program, Scientific Results* (Vol. 129, pp. 169-176). College Station, TX: Ocean Drilling Program.
- 736 Wagner, G. A. (1968). Fission track dating of apatites. *Earth and Planetary Science Letters*, 4(5), 411-415.
737 [https://doi.org/10.1016/0012-821X\(68\)90072-1](https://doi.org/10.1016/0012-821X(68)90072-1)
- 738 Wauschkuhn, B., Jonckheere, R., & Ratschbacher, L. (2015). The KTB apatite fission-track profiles: Building on a
739 firm foundation? *Geochimica et Cosmochimica Acta*, 167, 27-62. <https://doi.org/j.gca.2015.06.015>
- 740 Ziegler, J. F. (2013). SRIM-2013 The stopping and range of ions in matter. Annapolis: United States Naval
741 Academy. Retrieved from <http://www.srim.org/>
742